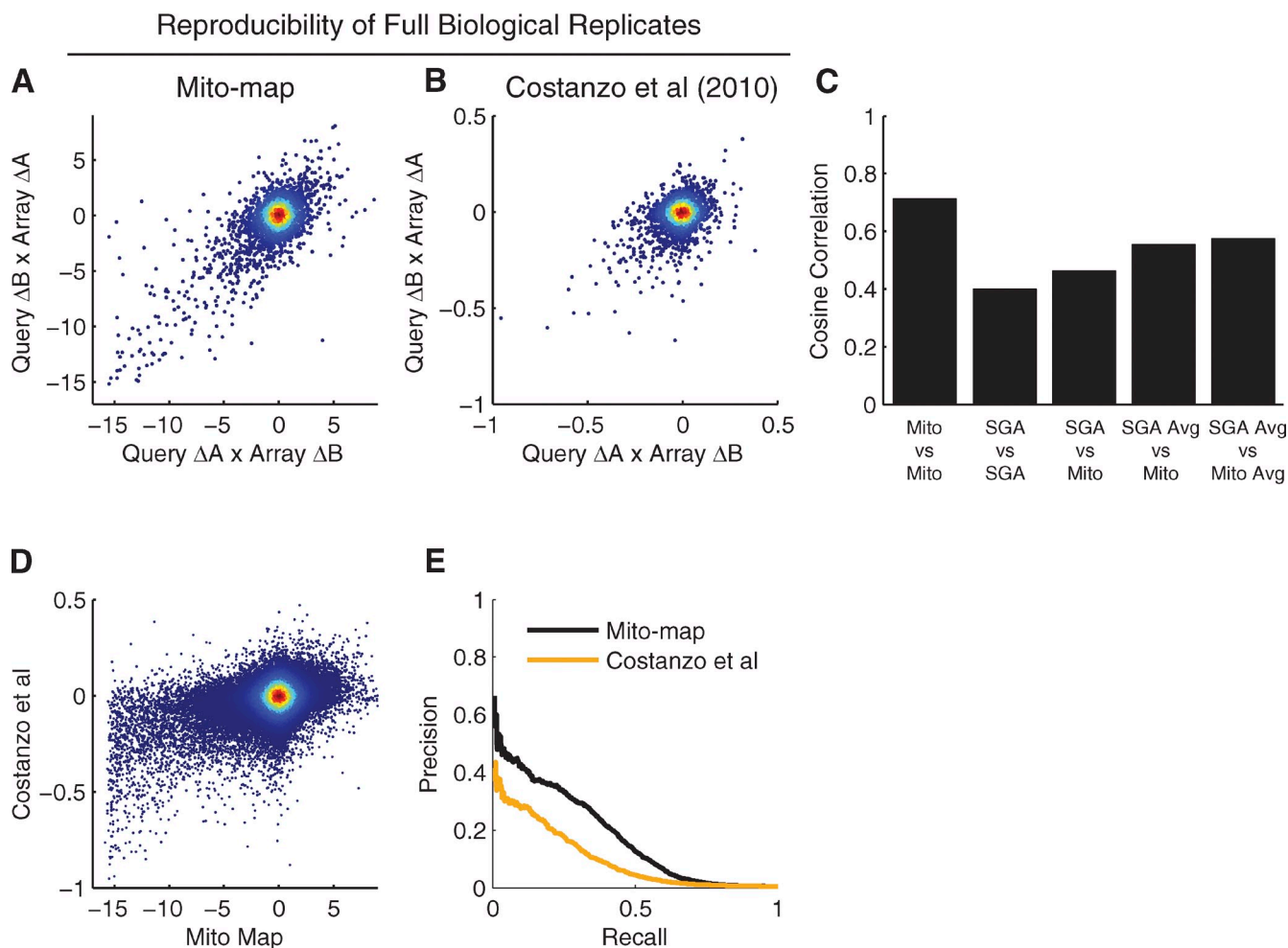Figure S1. **Internal agreement of MITO-MAP data and consistency with previously published interactions.** (A and B) The set of 5,616 mutation pairs that were measured for both possible double mutant strain constructions (Query ΔA x Array ΔB and Query ΔB x Array ΔA) in both the new MITO-MAP data (see Table S4) and the dataset from Costanzo et al. (2010) were used for a comparison of internal consistency. Each plot shows the genetic interaction measurements from the corresponding dataset for each of these mutation pairs from the two independent double mutant strain constructions. The Pearson correlation coefficients for these scatter plots is 0.71 (MITO-MAP) and 0.39 (Costanzo et al., 2010). (C) Shown is a bar graph of cosine correlation coefficients between different measures of the quantitative genetic interactions for the same 5,616 mutation pairs analyzed in A and B. Bars correspond to MITO-MAP measurement 1 (i.e., Query ΔA x Array ΔB) versus MITO-MAP measurement 2 (Query ΔB x Array ΔA), SGA (Costanzo et al., 2010) measurement 1 versus SGA measurement 2, SGA measurements versus MITO-MAP measurements, the mean of SGA measurement 1 and SGA measurement 2 versus MITO-MAP measurement 1, and the mean of SGA measurement 1 and SGA measurement 2 versus the mean of MITO-MAP measurement 1 and MITO-MAP measurement 2. (D) A density-colored scatter plot of individual genetic interaction score measurements from the MITO-MAP versus score measurements for the corresponding mutation pairs in the Costanzo et al. (2010) dataset, including all 262,332 mutation pairs analyzed in both studies. (E) A precision-recall plot measuring the ability of individual genetic interaction score measurements from the MITO-MAP and the corresponding measurements of the same mutation pairs from Costanzo et al. (2010) to recapitulate previously published synthetic genetic interactions. The reference set of synthetic genetic interactions were those annotated as phenotypic enhancement, synthetic growth defect, or synthetic lethality in the BioGRID database (release 3.1.72).
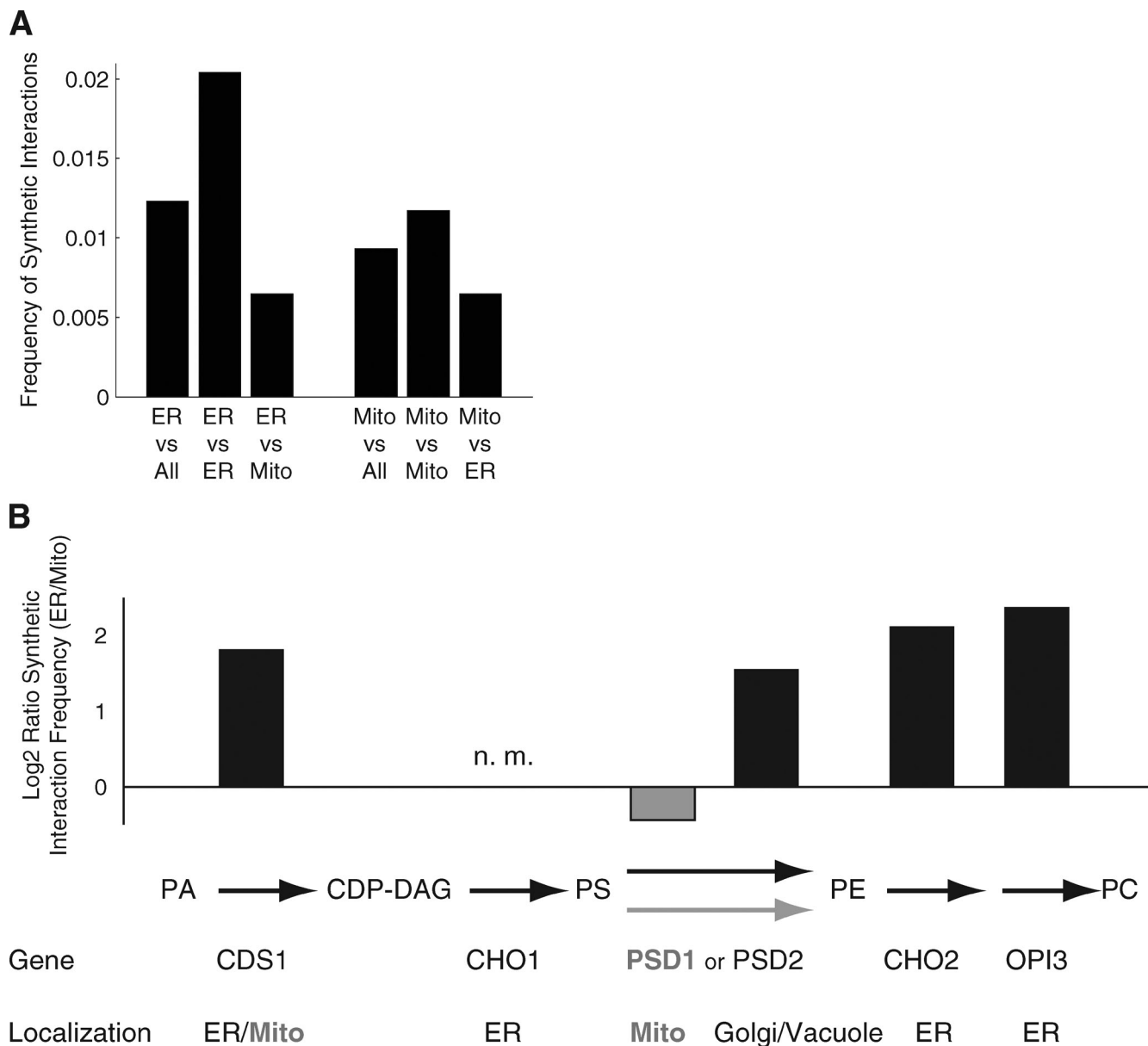
Figure S2. **MITO-MAP genetic interaction analysis.** (A) Frequency of synthetic genetic interactions between genes encoding mitochondrially and ER-localized proteins. Shown is a bar graph of the frequency of synthetic interactions in the MITO-MAP (score < −3) for pairs of mutations from genes encoding proteins localized to the ER, genes encoding proteins localized to the mitochondria, or all mutations in the MITO-MAP. Localization to the ER or mitochondria was based on either systematic results from yeast strains expressing GFP-tagged proteins (Kumar et al., 2002; Huh et al., 2003) or GOSlim component annotations (see Table S3). Genes annotated as being localized to both ER and mitochondria were excluded. (B) Relative frequency of synthetic genetic interactions between components of the phosphatidylcholine biosynthesis pathway with genes encoding ER or mitochondrially localized proteins. Shown is a bar graph of the $\log_2$ ratio of the synthetic interaction frequencies (score < −3) for each indicated gene with genes annotated as encoding ER versus mitochondrial proteins (annotations are the same as in Fig. S2 and are listed in Table S3). Included are the enzymes of the cytidine diphosphate diacylglycerol pathway of phosphatidylcholine biosynthesis. Also shown is the localization of each corresponding protein. Gene names and bars are colored according to protein localizations.
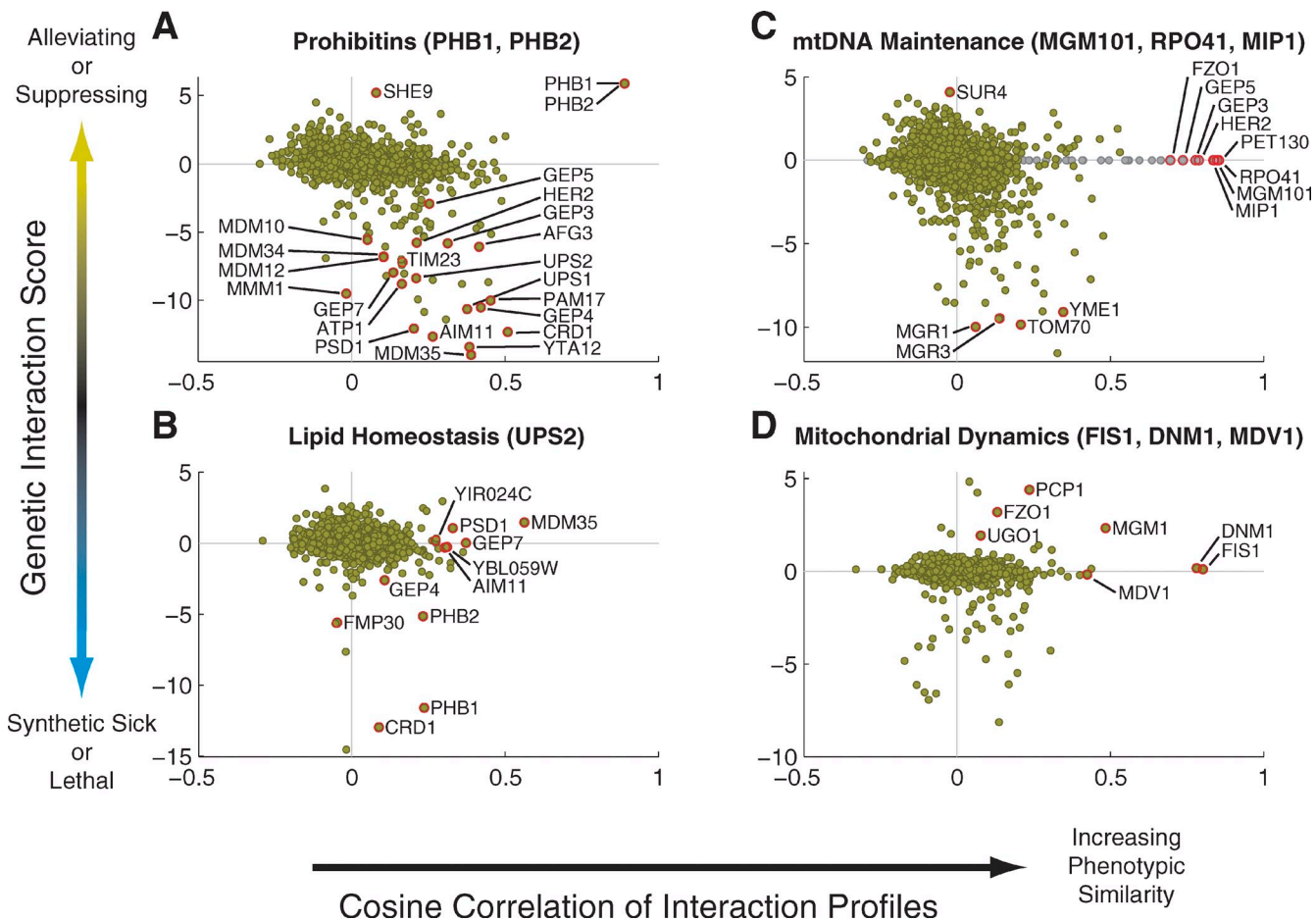
Figure S3. Genetic connection scatter plots highlight relationships for four aspects of mitochondrial biology. In each scatter plot, the x axis represents the cosine correlation between the mean of the interaction score vectors for the selected genes (those indicated in the title of the plot) and the interaction score vector for each gene in the MITO-MAP. The y axis indicates the mean interaction score between the selected genes and each gene in the MITO-MAP. Every point in the scatter plot represents one gene. The cosine correlation values for points corresponding to the selected genes themselves were computed using the mean of the interaction score vectors for the remaining selected genes. In cases where the genetic interaction score was not measured, the point is plotted in gray along the line y = 0. (A) The prohibitins PHB1 and PHB2. The prohibitins Phb1 and Phb2 function and assemble together in an interdependent manner into large oligomeric ringlike structures on the inner mitochondrial membrane, where they are known to associate with the m-AAA protease and modulate the rate of protein turnover within mitochondria (Steglich et al., 1999; Tatsuta et al., 2005). Consistent with this understanding, the genetic interaction profiles for *PHB1* and *PHB2* are very highly correlated, and the two genes have a strong positive genetic interaction. Both *PHB1* and *PHB2* interact with a relatively large set of genes in the MITO-MAP; these overlap to a significant degree with genes in the recently described prohibitin interactome generated from a synthetic genetic array analysis of Δ*phb1* cells (genes termed genetic interactors of prohibitin; GEP; Osman et al., 2009a). The exact function of *PHB1* and *PHB2* is currently not understood, but the prohibitin complex has been proposed to act as a scaffold that organizes inner membrane proteins and lipids (Osman et al., 2009a,b). Many of the interaction we observed are consistent with this model. Strong negative interactions are observed with GEP genes, genes encoding CL, biosynthetic (*CRD1* and *GEP4*) and PE biosynthetic (*PSD1*) enzymes, genes encoding components of the ERMES complex (*MDM10*, *MDM34*, *MDM12*, and *MMM1*), and genes encoding respiratory complex components (*ATP1*). *PHB1* and *PHB2* also have a high degree of correlation and a negative genetic interaction with *AFG3* and *YTA12*, which encode the interdependent components of the m-AAA protease, which is consistent with previous reports (Steglich et al., 1999). Interestingly, we observed a significant positive interaction with SHE9/MDM33, which encodes a transmembrane coiled-coil protein that may function to mediate inner membrane division (Messerschmitt et al., 2003). In addition to the previously identified GEP genes, we observed significant negative interactions with genes encoding inner membrane import machinery components (*TIM23* and *PAM17*). Two of the most highly correlated genes are *CRD1* and *GEP4*, which encode sequential CL biosynthetic enzymes; however, genes encoding outer membrane import components in the MITO-MAP also show significant correlation, which is indicative of a shared function. Thus, although our analysis supports the proposed central role for the prohibitin complex as a membrane scaffold that affects the organization of inner membrane proteins and phospholipids, it is more likely that it has a more global role in determining the structure and function of the organelle. (B) The regulator of mitochondrial lipid homeostasis UPS2. The prohibitin interactome also contained *UPS1* and *UPS2*, which encode conserved and homologous PRELI-like intermembrane space proteins. Ups1 and Ups2 function in a competitive manner in the intermembrane space to coordinate the abundance of the nonbilayer phospholipids CL and PE, respectively (Tamura et al., 2009; Potting et al., 2010). Coordination of non-bilayer CL and PE abundance is critical, as one lipid can at least partially compensate for the reduction in the other, but depletion of both CL and PE is lethal to cells (Gohil et al., 2005). Ups1 and -2 protein levels are key to their role in regulating CL and PE levels. Both Ups1 and Ups2 are stabilized via a direct interaction with the product of *MDM35*, an additional prohibitin interacting gene (Potting et al., 2010; Tamura et al., 2010). Indeed, the gene with the most correlated pattern to that of *UPS2* is *MDM35*, and both *UPS1* and *UPS2* have strong positive interactions with *MDM35*. Consistent with a role of *UPS2* in PE maintenance, it has a positive interaction and correlation with *PSD1* and negative genetic interactions with *CRD1*, *GEP4*, and *FMP30*, which encodes an inner membrane protein also recently shown to function in CL biosynthesis (Kuroda et al., 2011). Additionally, two pairs of poorly characterized genes (*AIM11*/*GEP8* and *YIR024c* as well as *GEP7* and *YBL059W*) emerge as outliers in the genetic connection scatter plot. The products of these genes are localized to mitochondria, their genetic interaction profiles are highly correlated with that of *UPS2*, and the profiles within each pair are highly correlated with each other. Thus these are two strong candidates for novel complexes involved in Ups2-regulated mitochondrial lipid homeostasis. (C) Genes encoding the three well-characterized components of the mitochondrial nucleoid in

the MITO-MAP: the catalytic subunit of the mitochondrial DNA polymerase (*MIP1*), the mitochondrial RNA polymerase (*RPO41*), and mitochondrial DNA repair factor *MGM101*. The MITO-MAP contains three well-characterized genes whose products perform key roles in mtDNA metabolism and maintenance in mitochondrial nucleoids: the conserved mitochondrial DNA and RNA polymerases, and *MGM101*, a gene encoding a protein with homology to Rad52 that is required for the repair and maintenance of mtDNA (Meeusen et al., 1999). The genetic interaction patterns for these genes are highly correlated, and so we used the average of their profiles as the basis for a genetic connection scatter plot to explore mitochondrial nucleoid biology. Genes previously identified as petite negative such as *YME1*, which encodes the i-AAA protease; and *MGR1* and *MGR3*, whose products are thought to function as i-AAA protease adaptors, have significant negative interactions with the nucleoid cluster, but their patterns are not highly correlated (Dunn et al., 2006). However, several other genes with interaction patterns highly similar to those of the nucleoid genes are apparent. These include *PET130* and *GEP5*, which are poorly characterized genes required for respiratory growth and maintenance of CL and PE levels, respectively; and *HER2/GEP6* and *GEP3/AIM30*, which encode genes that are likely to be involved in aspects of mitochondrial protein translation. Indeed, *GEP3* encodes a GTPase that is conserved across bacteria and eukaryotes, including humans, and in bacteria functions in ribosome biogenesis. This latter pair of genes is consistent with the observation that the mitochondrial translation machinery is intimately linked to and required for mtDNA maintenance. Thus, these genes encode strong candidates for proteins that function in the maintenance mtDNA. (D) Genes encoding the core components of the mitochondrial fission machinery FIS1, DNM1, and MDV1. The *DNM1*, *MDV1*, and *FIS1* genes encode the core components of the mitochondrial division pathway. Consistent with this primary role, the genetic interaction patterns for these genes are highly correlated. Four of the strongest positive interactions with the division genes are with *FZO1*, *MGM1*, *PCP1*, and *UGO1*, which is expected from their roles in the opposing process of mitochondrial fusion. Interestingly, the patterns of interaction for the mitochondrial fusion genes differ substantially, despite the fact that their products physically interact and function together in a common pathway. However, unlike the division components that function at the outer mitochondrial membrane exclusively, the core dynamin-related fusion components, Fzo1 and Mgm1, are localized to the outer and inner membranes, respectively, where they mediate sequential but separable membrane fusion events (Meeusen et al., 2004, 2006). Thus, the MITO-MAP analysis is consistent with the idea that outer and inner membrane fusion events have different functional consequences and/or that the fusion genes perform additional diverse functions in the cell. It is therefore interesting to note that that the pattern for *FZO1* is highly correlated with those of the nucleoid genes, which is consistent with its role in the maintenance of mtDNA; in contrast, *MGM1* has a high correlation with mitochondrial division genes. This close correlation is potentially consistent with data suggesting a role for Mgm1 in the generation of inner membrane cristae structures (Meeusen et al., 2006). In this context, the division machine might also function to produce an inner membrane–only division event to generate a mitochondrion with a continuous outer membrane that encapsulates opposed mitochondrial inner membranes belonging to separate matrices. This mitochondrial structure is topologically equivalent to the product of an outer membrane fusion event. Mgm1-dependent fusion of opposing inner membranes in this structure could generate cristae, raising the possibility that the inner membrane fusion and outer membrane division machines collaborate to control mitochondrial inner membrane structure.

A

(scatter plot)

Y-axis: YGR235C (range −10 to 5)
X-axis: AIM5, AIM13, FCJ1, AIM37 (range −10 to 5)

B

T	A		% total adsorbed
		Aim5 FLAG (12 kD)	18
		Fcj1 HA (61 kD)	13
		Aim13 HA (19 kD)	22.5
		Aim37 HA (27 kD)	21

C

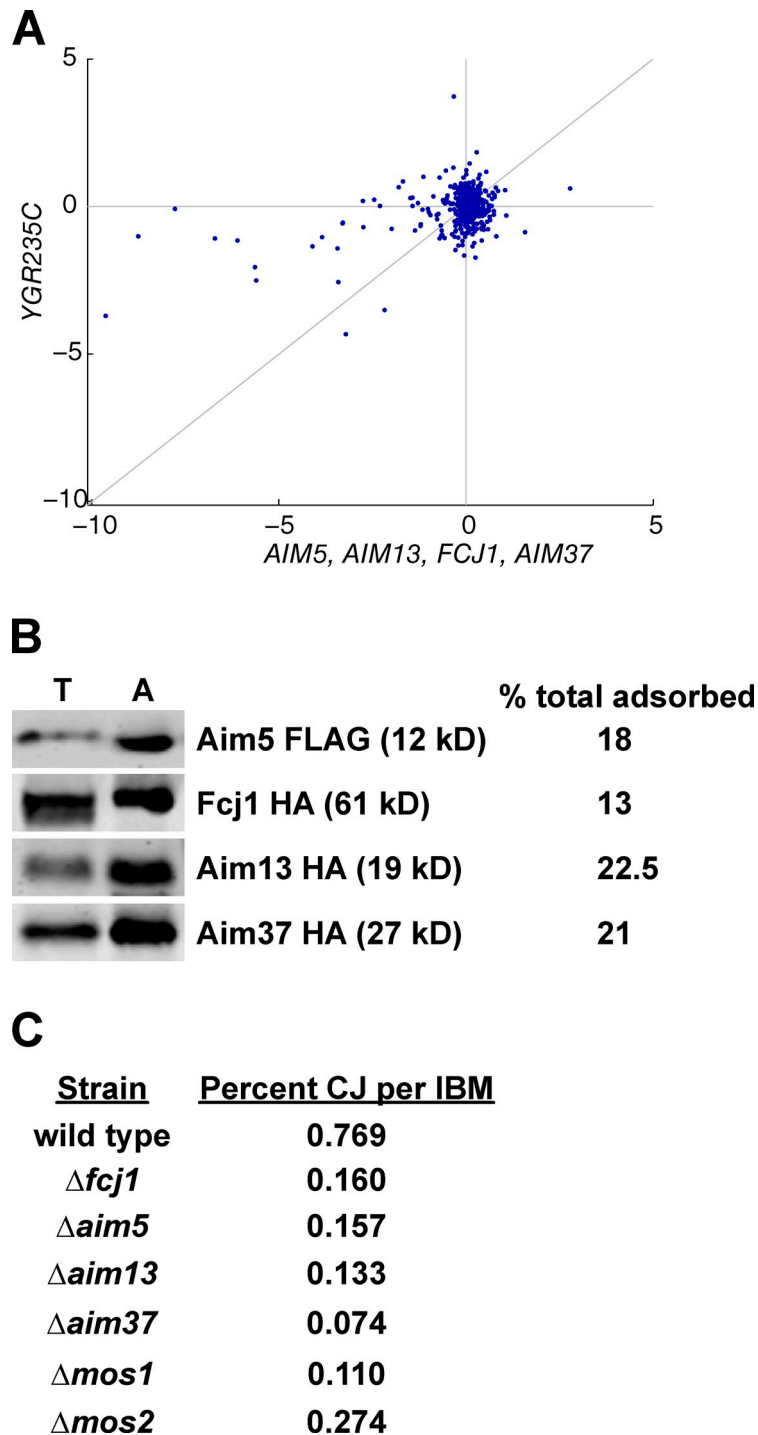| Strain	Percent CJ per IBM
wild type	0.769
Δ*fcj1*	0.160
Δ*aim5*	0.157
Δ*aim13*	0.133
Δ*aim37*	0.074
Δ*mos1*	0.110
Δ*mos2*	0.274

Figure S4.   **Scatter plot of YGR235c with genes encoding MitOS components, analysis of FLAG purification, and quantification of cristae junctions in cells lacking components of MitOS.** (A) A scatter plot is shown of the mean genetic interaction score of Δ*aim5*, Δ*aim13*, Δ*fcj1*, and Δ*aim37*, with each mutation in the MITO-MAP versus the corresponding scores for Δ*ygr235c/mos2*. (B) Western analysis of FLAG-tag purification. Aim5-FLAG purification was performed as described in Materials and methods except that the adsorbed proteins were eluted with sample buffer rather than performing the on-bead digest. The proteins were subject to SDS-PAGE and Western analysis with either α-FLAG or α-HA monoclonal antibodies. T, total; A, absorbed. (C) To quantify the abundance of cristae junctions, we randomly picked and photographed 50 mitochondrial cross sections for each strain. To correct for differences in size and shape of mutant mitochondria, we determined the perimeter of each organelle and related the numbers of identified cristae junctions to the length of the inner boundary membrane (IBM). We found that the relative number of cristae junctions was reduced almost threefold for Δ*mos2*, and five- to tenfold for Δ*aim5*, Δ*aim13*, Δ*aim37*, Δ*fcj1*, and Δ*mos1* in comparison to the wild type.
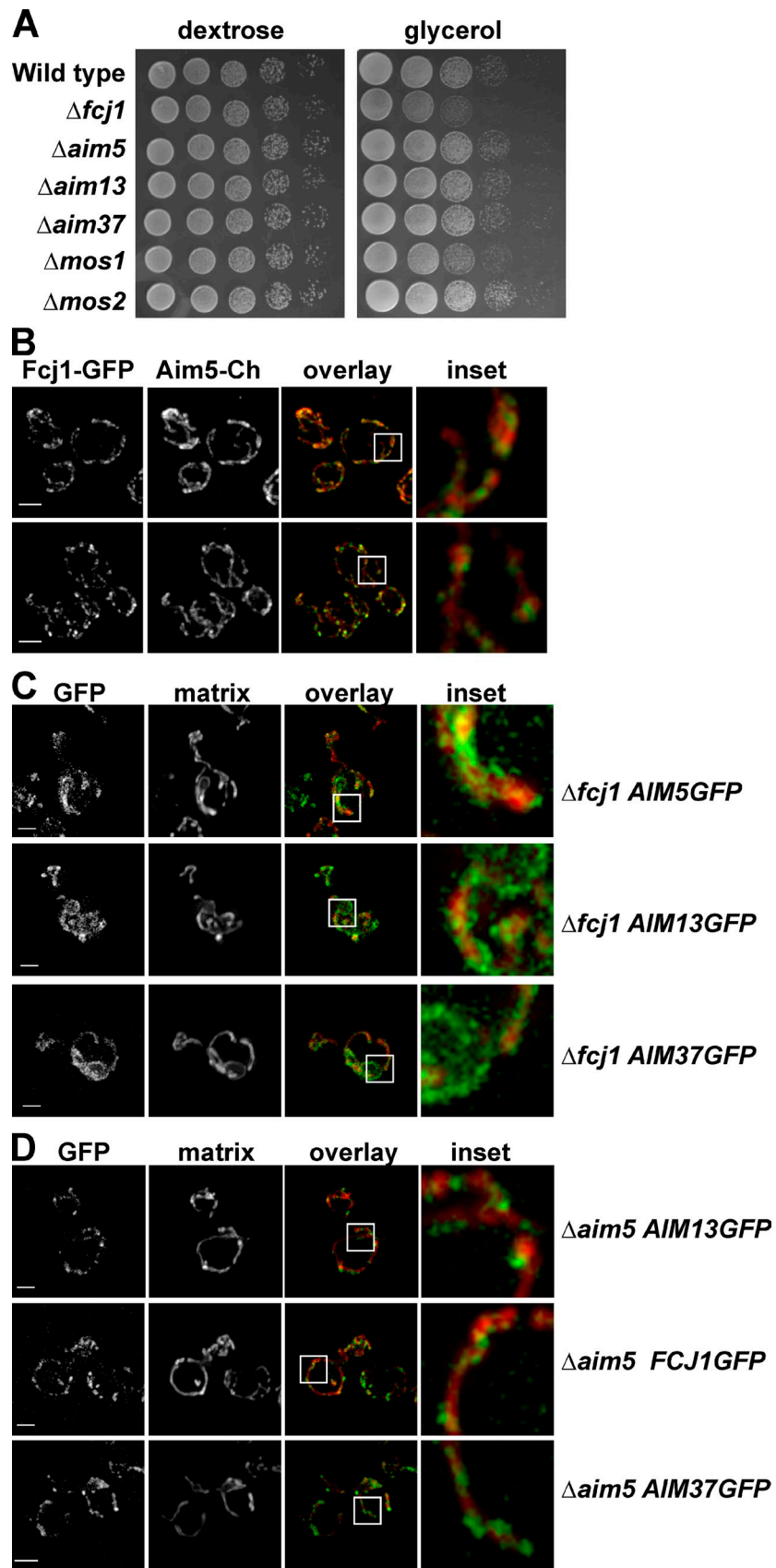
Figure S5. **Analysis of cells lacking MitOS components and colocalization of Fcj1 and Aim5.** (A) Growth analysis of cells lacking components of MitOS. Serial dilutions of the indicated deletion strains plated on SD-glycerol media and grown at 30°C. (B) Colocalization of Fcj1-yeGFP and Aim5-yEmCherry. Cells coexpressing fluorescently tagged versions of Fcj1 and Aim5 were visualized by light microscopy. Representative images are shown. The boxes indicate the areas shown in the insets. (C) Δ*fcj1* cells expressing GFP tagged versions of Aim5, Aim13, and Aim37 and mito-dsRed were visualized by light microscopy. Representative images are shown. The boxes indicate the areas shown in the insets. (D) Δ*aim5* cells expressing GFP-tagged versions of Aim5, Aim13, Aim37, and mito-dsRed were visualized by light microscopy. Representative images are shown. The boxes indicate the areas shown in the insets. Bars, 2 µm.
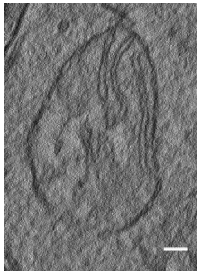
Video 1. **EM tomogram of a chemically fixed wild-type yeast cell.** Samples were examined in a JEM-2100 (JEOL Ltd.) or a CEM 902 (Carl Zeiss) transmission electron microscope operated at 80 kV. Successive xy slices through the tomogram are shown moving along the tomographic z axis. The video is shown at 15 frames/s; each frame is 1 nm in the z axis. Bar, 100 nm.

Video 2. **EM tomogram of a chemically fixed Δ*aim37* cell.** Samples were examined in a JEM-2100 (JEOL Ltd.) or a CEM 902 (Carl Zeiss) transmission electron microscope operated at 80 kV. Successive xy slices through the tomogram are shown moving along the tomographic z axis. The video is shown at 15 frames/s; each frame is 1 nm in the z axis. These images were used to measure cristae junctions in Fig. 5 D. Bar, 100 nm.

Video 3. **EM tomogram of a chemically fixed Δ*aim37* cell.** Samples were examined in a JEM-2100 (JEOL Ltd.) or a CEM 902 (Carl Zeiss) transmission electron microscope operated at 80 kV. Successive xy slices through the tomogram are shown moving along the tomographic z axis. The video is shown at 15 frames/s; each frame is 1 nm in the z axis. Bar, 100 nm.

Video 4. **EM tomogram of a chemically fixed Δ*aim5* cell.** Samples were examined in a JEM-2100 (JEOL Ltd.) or a CEM 902 (Carl Zeiss) transmission electron microscope operated at 80 kV. Successive xy slices through the tomogram are shown moving along the tomographic z axis. The video is shown at 15 frames/s; each frame is 1 nm in the z axis. These images were used to measure cristae junctions in Fig. 5 D. Bar, 100 nm.

Tables S1–S3 are available as Excel files.

Table S4 contains tab-delineated data and is available as a text file.

Java Treeview files are available in a ZIP file.

References

Costanzo, M., A. Baryshnikova, J. Bellay, Y. Kim, E.D. Spear, C.S. Sevier, H. Ding, J.L. Koh, K. Toufighi, S. Mostafavi, et al. 2010. The genetic landscape of a cell. *Science*. 327:425–431. http://dx.doi.org/10.1126/science.1180823

Dunn, C.D., M.S. Lee, F.A. Spencer, and R.E. Jensen. 2006. A genomewide screen for petite-negative yeast strains yields a new subunit of the i-AAA protease complex. *Mol. Biol. Cell*. 17:213–226. http://dx.doi.org/10.1091/mbc.E05-06-0585

Gohil, V.M., M.N. Thompson, and M.L. Greenberg. 2005. Synthetic lethal interaction of the mitochondrial phosphatidylethanolamine and cardiolipin biosynthetic pathways in Saccharomyces cerevisiae. *J. Biol. Chem.* 280:35410–35416. http://dx.doi.org/10.1074/jbc.M505478200

Huh, W.K., J.V. Falvo, L.C. Gerke, A.S. Carroll, R.W. Howson, J.S. Weissman, and E.K. O'Shea. 2003. Global analysis of protein localization in budding yeast. *Nature*. 425:686–691. http://dx.doi.org/10.1038/nature02026

Kumar, A., S. Agarwal, J.A. Heyman, S. Matson, M. Heidtman, S. Piccirillo, L. Umansky, A. Drawid, R. Jansen, Y. Liu, et al. 2002. Subcellular localization of the yeast proteome. *Genes Dev.* 16:707–719. http://dx.doi.org/10.1101/gad.970902

Kuroda, T., M. Tani, A. Moriguchi, S. Tokunaga, T. Higuchi, S. Kitada, and O. Kuge. 2011. FMP30 is required for the maintenance of a normal cardiolipin level and mitochondrial morphology in the absence of mitochondrial phosphatidylethanolamine synthesis. *Mol. Microbiol.* 80:248–265. http://dx.doi.org/10.1111/j.1365-2958.2011.07569.x

Meeusen, S., Q. Tieu, E. Wong, E. Weiss, D. Schieltz, J.R. Yates, and J. Nunnari. 1999. Mgm101p is a novel component of the mitochondrial nucleoid that binds DNA and is required for the repair of oxidatively damaged mitochondrial DNA. *J. Cell Biol.* 145:291–304. http://dx.doi.org/10.1083/jcb.145.2.291

Meeusen, S., J.M. McCaffery, and J. Nunnari. 2004. Mitochondrial fusion intermediates revealed in vitro. *Science*. 305:1747–1752. http://dx.doi.org/10.1126/science.1100612

Meeusen, S., R. DeVay, J. Block, A. Cassidy-Stone, S. Wayson, J.M. McCaffery, and J. Nunnari. 2006. Mitochondrial inner-membrane fusion and crista maintenance requires the dynamin-related GTPase Mgm1. *Cell*. 127:383–395. http://dx.doi.org/10.1016/j.cell.2006.09.021

Messerschmitt, M., S. Jakobs, F. Vogel, S. Fritz, K.S. Dimmer, W. Neupert, and B. Westermann. 2003. The inner membrane protein Mdm33 controls mitochondrial morphology in yeast. *J. Cell Biol.* 160:553–564. http://dx.doi.org/10.1083/jcb.200211113

Osman, C., M. Haag, C. Potting, J. Rodenfels, P.V. Dip, F.T. Wieland, B. Brügger, B. Westermann, and T. Langer. 2009a. The genetic interactome of prohibitins: coordinated control of cardiolipin and phosphatidylethanolamine by conserved regulators in mitochondria. *J. Cell Biol.* 184:583–596. http://dx.doi.org/10.1083/jcb.200810189

Osman, C., C. Merkwirth, and T. Langer. 2009b. Prohibitins and the functional compartmentalization of mitochondrial membranes. *J. Cell Sci.* 122:3823–3830. http://dx.doi.org/10.1242/jcs.037655

Potting, C., C. Wilmes, T. Engmann, C. Osman, and T. Langer. 2010. Regulation of mitochondrial phospholipids by Ups1/PRELI-like proteins depends on proteolysis and Mdm35. *EMBO J.* 29:2888–2898. http://dx.doi.org/10.1038/emboj.2010.169

Steglich, G., W. Neupert, and T. Langer. 1999. Prohibitins regulate membrane protein degradation by the m-AAA protease in mitochondria. *Mol. Cell. Biol.* 19:3435–3442.

Tamura, Y., T. Endo, M. Iijima, and H. Sesaki. 2009. Ups1p and Ups2p antagonistically regulate cardiolipin metabolism in mitochondria. *J. Cell Biol.* 185:1029–1045. http://dx.doi.org/10.1083/jcb.200812018

Tamura, Y., M. Iijima, and H. Sesaki. 2010. Mdm35p imports Ups proteins into the mitochondrial intermembrane space by functional complex formation. *EMBO J.* 29:2875–2887. http://dx.doi.org/10.1038/emboj.2010.149

Tatsuta, T., K. Model, and T. Langer. 2005. Formation of membrane-bound ring complexes by prohibitins in mitochondria. *Mol. Biol. Cell*. 16:248–259. http://dx.doi.org/10.1091/mbc.E04-09-0807